Meneses, J., García-Prada, J. C., Castejón, C., Rubio, H. & Corral, E. (2017). The kinematics of the rotary into helical gear transmission. *Mechanism and Machine Theory, vol. 108*, pp. 110–122.

DOI: 10.1016/j.mechmachtheory.2016.10.017

The kinematics of the rotary into helical gear transmission

Jesús Meneses, Juan Carlos García-Prada, Cristina Castejón, Higinio Rubio, Eduardo Corral

menses@ing.uc3m.es, jcgprada@ing.uc3m.es, castejon@ing.uc3m.es, hrubio@ing.uc3m.es, ecorral@ing.uc3m.es

Universidad Carlos III de Madrid. Calle Butarque, 15. 28911 Leganés (Madrid) Spain.

Abstract

A higher kinematic pair that converts rotary motion into helical motion is presented as an alternative to the screw joint (a lower kinematic pair). First, the existence of a rolling transmission pair for a rotary-to-helical motion conversion is proven. Then, the corresponding pair of rolling surfaces (pitch surfaces) and their relative position is defined for any set of kinematic transmission parameters. Some calculated examples are presented. A method for gear-tooth forming from the pitch surfaces using Boolean operations with a computer-aided design (CAD) program is proposed. Finally, applying this methodology, a pair of gears for rotary into helical transmission has been obtained using a 3D printer. The prototype presents negligible clearances and backlash, high reversibility, as well as continuous gearing without interference. The meshing equation for a simple generating surface is also provided.

Keywords: Higher kinematic pair, Pitch surfaces, Gear transmission, Rotary-helical motion transmission, Meshing Equation

1. Introduction

On rotary into helical transmission, the literature is very little, if any. In fact, helical motion is historically achieved by any kind of combination of a linear actuator with a rotary actuator, or by a low order kinematic pair (screw joint), where the friction is not negligible, such as that described in the Thomas A. Edison's phonograph design [1]. But the truth is that no published work on rotary into helical transmission by gears has been found by the authors.

Actually, the motivation of this work comes from a patented mechanism "Dispositivo Automático para Biopsias Cutáneas (Automatic Device for Skin Biopsy)" [2] for generating helical motion with a single actuation. The performance of this device worsens to the extent that actual slipping occurs in the kinematic pair it is based on, and could be improved by the rotary-helical transmission presented in this work.

A mechanism partly equivalent to that proposed in this manuscript is the patented "Adjustable Angle Helix Generator for Edge and Radial Relief Sharpening" [3]. In the opinion of the authors, the disadvantage of this mechanism is that it is based on a rather weak rotary-helical transmission kinematic pair, since it is provided by a point contact rolling between non-parallel cylinders. A similar mechanism, but having the gear transmission kinematic pair proposed it this paper, could lead considerably more thrust.

The "spiral motor" [4]-[7] is an actuator that produces helical motion, but it is used primarily as a linear actuator (see [5] or [6], for example). However, in [7], a two degrees of freedom induction motor prototype with rotor helical motion, "suitable for several industrial applications as grinders, augers, drilling and milling spindles, robotic arms and drives for medical tools and prostheses", is described. In this respect, the transmission mechanism proposed here shares the latter applications, and it could also be used as a rotary-linear transmission. Additionally, new geometries such as those proposed in this article could be considered in the design of linear actuators based on electromagnetic gears and/or helical electromagnetic motors, which can provide a wide future line of research.

Gear mechanisms are commonly used to transform rotary motion into either rotary or linear motion. In rotary-to-rotary-motion transmissions, where both axes are parallel or intersecting, it is easy to obtain the corresponding pair of rolling contact surfaces (pitch surfaces); they are their axodes. These are two cylinders and two cones, respectively, having either the diameter ratio or the cone base diameter ratio equal to the transmission ratio. Conversely, no set of rolling surfaces exists for transmission between two skew axes (i.e., non-parallel and non-intersecting) since their axodes do not roll without sliding. However, the operating pitch surfaces are defined for gears with crossed axes [8],[9]. Based on these pitch surfaces (either cylinders or cones), helical or spiral gears can be used for any two crossed axes at any angle, by a suitable choice of helix angle, in addition to worm and hypoid gears for the case of axes crossed at a right angle.

This paper addresses the existence of a pair of rolling surfaces for transmitting rotary motion into helical motion between crossed axes, at any distance and angle between them. The method of tooth-generation on these surfaces in order to obtain a rotary-helical transmission is also considered.

2. A Rolling Kinematic Pair for the Rotary to Helical Transmission. Pitch Surfaces.

In this section two rigid solids are considered: one performing a pure rotation (body 1), and the other performing a helical motion (body 2). It is shown that, i) for any set of values of their angular velocities, ii) for any value of the helical linear velocity of body 2, and iii) for any orientation of the corresponding axes relative to each other; there is a line where the velocity fields corresponding to each body are equal. Therefore, a pair of ruled surfaces (each one attached to each

body) exists such that each rolls, without slipping, on the other. These are the so-called pitch surfaces for the rotary into helical transmission.

Without loss of generality, we will consider the helical motion of body 2 around the z-axis. The motion is then characterized by the following linear and angular velocities, respectively:

$$\vec{v} = v\vec{k} \tag{1a}$$

$$\vec{\omega}_2 = \omega_2\vec{k} \tag{1b}$$

Meanwhile, body 1 rotates around the R-axis, which lies in a plane defined by $x = d$, and is parallel to the y-z plane (see Fig.1), so that its angular velocity can be expressed as equation (2).

$$\vec{\omega}_1 = \omega_{1_y}\vec{j} + \omega_{1_z}\vec{k} \tag{2}$$

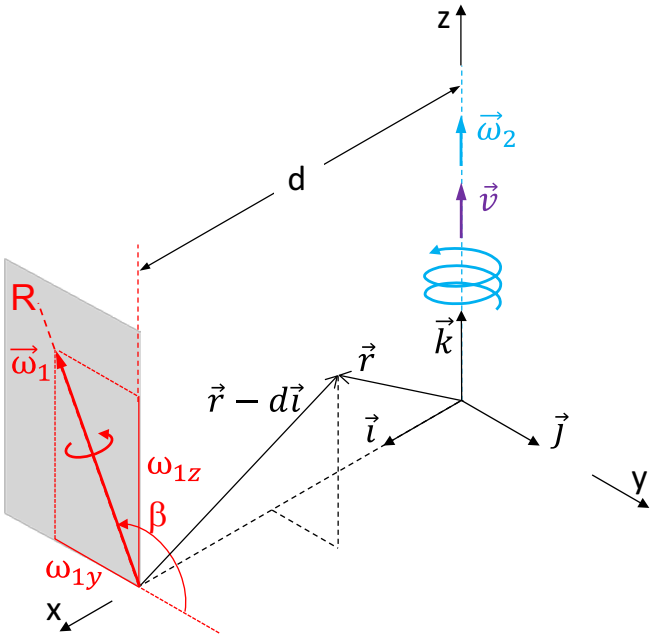

Fig. 1 The kinematic and geometric parameters of the rotary-to-helical motion transmission.

Let $\vec{r} = x\vec{\imath} + y\vec{\jmath} + z\vec{k}$ be the position vector for a generic point. If this point belongs to body 2 (helical motion) its velocity can be expressed as equation (3), which is the velocity field of body 2.

$$\vec{v}_2(\vec{r}) = \vec{v} + \vec{\omega}_2 \times \vec{r} = -\omega_2 y\vec{\imath} + \omega_2 x\vec{\jmath} + v\vec{k} \tag{3}$$

The velocity field of body 1 can be written as

$$\vec{v}_1(\vec{r}) = \vec{\omega}_1 \times (\vec{r} - d\vec{\imath}) = \left[\omega_{1_y} z - \omega_{1_z} y\right]\vec{\imath} + \omega_{1_z}(x - d)\vec{\jmath} - \omega_{1_y}(x - d)\vec{k} \tag{4}$$

Equating both these velocities, the subspace of points having the same velocity in both solids is thus obtained:

$$\vec{v}_1(\vec{r}) = \vec{v}_2(\vec{r}) \Rightarrow \begin{cases} (\omega_2 - \omega_{1_z})y + \omega_{1_y} z = 0 \\ (\omega_2 - \omega_{1_z})x = -d \cdot \omega_{1_z} \\ \omega_{1_y} x = d \cdot \omega_{1_y} - v \end{cases} \tag{5}$$

These points are referred to as “rolling points”. These equations can be succinctly expressed in matrix form as:

$$\begin{pmatrix} 0 & \omega_2 - \omega_{1_z} & \omega_{1_y} \\ \omega_2 - \omega_{1_z} & 0 & 0 \\ \omega_{1_y} & 0 & 0 \end{pmatrix} \begin{pmatrix} x \\ y \\ z \end{pmatrix} = \begin{pmatrix} 0 \\ -d \cdot \omega_{1_z} \\ d \cdot \omega_{1_y} - v \end{pmatrix} \tag{6}$$

Now we will discuss the existence of solutions of this system of equations using to the Rouché-Capelli theorem [10]. The system matrix and the extended matrix can be referred to as (A) and (A|B) respectively, and are:

$$(A) = \begin{pmatrix} 0 & \omega_2 - \omega_{1_z} & \omega_{1_y} \\ \omega_2 - \omega_{1_z} & 0 & 0 \\ \omega_{1_y} & 0 & 0 \end{pmatrix} \tag{7a}$$

$$(\mathrm{A}|\mathrm{B}) = \left(\begin{array}{ccc|c} 0 & \omega_2 - \omega_{1_z} & \omega_{1_y} & 0 \\ \omega_2 - \omega_{1_z} & 0 & 0 & -\mathrm{d}\cdot\omega_{1_z} \\ \omega_{1_y} & 0 & 0 & \mathrm{d}\cdot\omega_{1_y} - \mathrm{v} \end{array}\right) \tag{7b}$$

Since the determinant of the matrix (A) is always zero, if a solution exists it will therefore not be unique. In fact, the system will be consistent (i.e., undetermined) if and only if rank (A) = rank (A|B), and its set of solutions will either be the whole space $\mathbb{R}^3$, a plane or a line, corresponding to rank values of 0, 1 or 2, respectively. The system will be inconsistent if rank (A) ≠ rank (A|B). The consistent solutions are now discussed by case:

i) If $\omega_{1_z} = \omega_2$ and $\omega_{1_y} = 0$, then rank (A) = 0. Rank (A|B) is also equal to zero, but only if $v = 0$ and either$\left(d = 0 \text{ or } \omega_{1_z} = 0\right)$. This is a trivial solution: no relative motion between both bodies exists.

ii) rank (A) ≠ 1, since $(A)^T = (A)$ and the principal diagonal elements are all zero: if any element of (A) is not zero, then neither is its diagonaly symmetrical element, and a non-zero second order determinant results.

iii) If either or both $\left(\omega_{1_z} \neq \omega_2 \text{ or } \omega_{1_y} \neq 0\right)$, then rank (A) = 2. Rank (A|B) is also equal to 2 (the solution points form a straight line), but only if the following equations are simultaneously fulfilled:

$$\left|\begin{array}{ccc} 0 & \omega_2 - \omega_{1_z} & 0 \\ \omega_2 - \omega_{1_z} & 0 & -\mathrm{d}\cdot\omega_{1_z} \\ \omega_{1_y} & 0 & \mathrm{d}\cdot\omega_{1_y} - \mathrm{v} \end{array}\right| = 0 \Rightarrow \left(\omega_2 - \omega_{1_z}\right)\left[\mathrm{d}\cdot\omega_{1_y}\omega_{1_z} + \left(\omega_2 - \omega_{1_z}\right)\left(\mathrm{d}\cdot\omega_{1_y} - \mathrm{v}\right)\right] = 0 \tag{8a}$$

$$\left|\begin{array}{ccc} 0 & \omega_{1_y} & 0 \\ \omega_2 - \omega_{1_z} & 0 & -\mathrm{d}\cdot\omega_{1_z} \\ \omega_{1_y} & 0 & \mathrm{d}\cdot\omega_{1_y} - \mathrm{v} \end{array}\right| = 0 \Rightarrow \omega_{1_y}\left[\mathrm{d}\cdot\omega_{1_y}\omega_{1_z} + \left(\omega_2 - \omega_{1_z}\right)\left(\mathrm{d}\cdot\omega_{1_y} - \mathrm{v}\right)\right] = 0 \tag{8b}$$

Note that the determinant of the remaining third order submatrix in (A|B) is always equal to zero.

Equations (8) are fulfilled simultaneously for $\left(\omega_{1_z} \neq \omega_2 \text{ or } \omega_{1_y} \neq 0\right)$ if and only if:

$$\mathrm{d}\cdot\omega_{1_y}\omega_{1_z} + \left(\omega_2 - \omega_{1_z}\right)\left(\mathrm{d}\cdot\omega_{1_y} - \mathrm{v}\right) = 0 \tag{9}$$

If the translation velocity v is zero, then equations (8) are fulfilled only if $\omega_2 = 0$, i.e., no transmission exists. However, if body 1 performs a strictly helical motion, with $\omega_2 \neq 0$ and $v \neq 0$, then a straight line of points having the same velocity on both solids exists so long as condition (9) is met. This line would be the contact line between the rolling surfaces in the rotary-to-helical motion transmission. In fact the parameters that characterize the transmission, v, ω_2, ω_{1_y}, ω_{1_z} and d, are not independent, but interrelated by (9). For instance, we can express d in terms of the other four parameters. By replacing components ω_{1_y} and ω_{1_z} by $\omega_1 \cos\beta$ and $\omega_1 \sin\beta$ respectively (see Fig.1), (9) yields:

$$\mathrm{d} = \frac{\mathrm{v}(\omega_2 - \omega_1 \sin\beta)}{\omega_2 \omega_1 \cos\beta} \tag{10}$$

The contact line (or "rolling line") is then obtained by solving the system of equation in (5) whilst observing the restriction given in (10). This leads to

$$\begin{cases} \frac{\mathrm{z}}{\mathrm{y}} \equiv \tan\vartheta = \tan\beta - \frac{\omega_2}{\omega_1 \cos\beta} & \text{(a)} \\ \mathrm{x} = -\frac{\mathrm{v}}{\omega_2}\tan\beta & \text{(b)} \end{cases} \tag{11}$$

Equation (11b) indicates that the rolling line is also parallel to the y-z plane, and at a non-zero distance which is dependent on the direction angle between axes, as well as on the ratio v/ω_2. In equation (11a), the angle ϑ defines the direction of the rolling line, which depends on the angle between axes, β, and on the ratio ω_2/ω_1. The rolling line is shown in fig. 2.

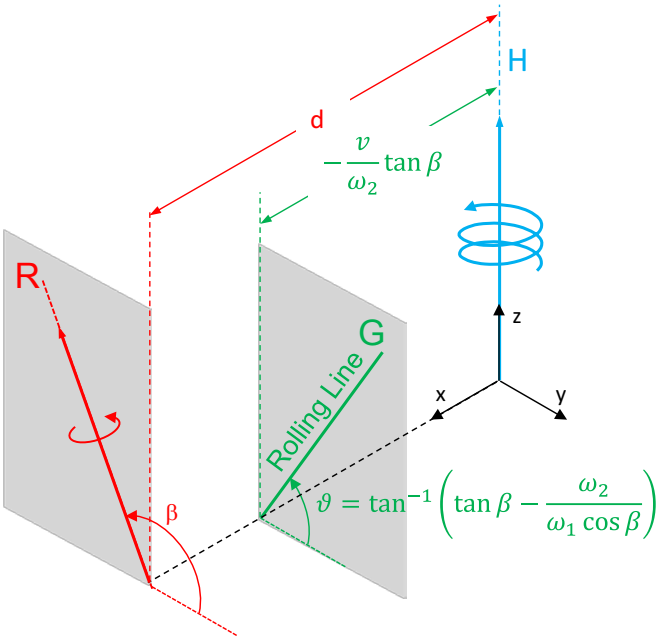

Fig. 2. The position of rolling line G, with respect to rotary axis R and helical axis H, which depends on the transmission parameters (β,ω_1,ω_2 and v).

Therefore, both rolling surfaces are ruled surfaces and tangent to each other along the common generatrix line (G in Fig. 2) defined by equation (11).

The pitch surface corresponding to the pure rotating motion is the hyperboloid generated by rotating the generatrix G about the R-axis, their s,t-parametric equations being (as derived in the Appendix):

$$\begin{cases} x_{s,t} = v\left(\frac{1-\cos\omega_1 t}{\omega_1 \cos\beta} - \frac{\tan\beta}{\omega_2}\right) - s\frac{\omega_2}{\omega_1}\sin\omega_1 t \\ y_{s,t} = -\frac{v}{\omega_1}\tan\beta\sin\omega_1 t + s\left[1 + \frac{\omega_2}{\omega_1}\sin\beta\,(\cos\omega_1 t - 1)\right] \\ z_{s,t} = \frac{v}{\omega_1}\sin\omega_1 t + s\left[\tan\beta - \frac{\omega_2}{\omega_1}\cos\beta\,(\cos\omega_1 t + \tan^2\beta)\right] \end{cases} \quad (12)$$

By varying s, different points of the generatrix are obtained; whereas varying t involves generatrix rotation about R-axis.

The pitch surface corresponding to the helical motion is a ruled z-axis helicoid, which is shaped by the generatrix line G describing that helical motion. Hence their s,t-parametric equations are

$$\begin{cases} x_{s,t} = -\frac{v}{\omega_2}\tan\beta\cos\omega_2 t - s\sin\omega_2 t \\ y_{s,t} = -\frac{v}{\omega_2}\tan\beta\sin\omega_2 t + s\cos\omega_2 t \\ z_{s,t} = s\left(\tan\beta - \frac{\omega_2}{\omega_1\cos\beta}\right) + vt \end{cases} \quad (13)$$

These are derived in the Appendix. In Fig. 3, both pitch surfaces are represented.

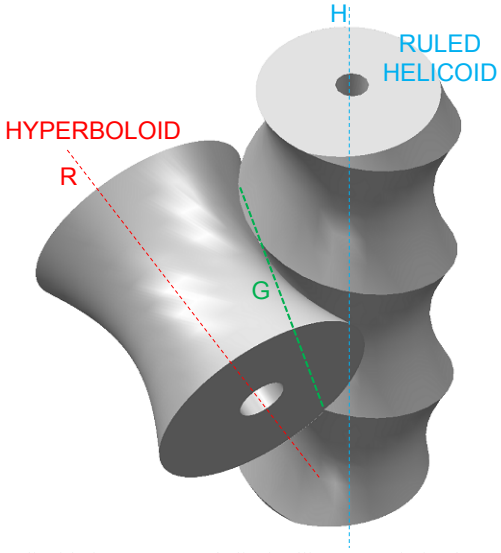

Fig. 3. The ruled pitch surfaces –Hyperboloid and Helicoid- for a rotary-to-helical rolling transmission between axes R and H respectively. The common generatrix G has been also depicted.

Equations (10) to (13) have been implemented in MATLAB® code in order to plot the pitch surfaces for any value of the transmission parameters, as well as the corresponding geometric parameters. These are the hyperboloid and helicoid throat radii, r_1 and r_2 respectively in equation (14); and the semi-length l of the generatrix (for both pitch surfaces).

$$r_1 = \left|d + \frac{v}{\omega_2}\tan\beta\right| = \left|\frac{v}{\omega_1 \cos\beta}\right| \tag{14a}$$

$$r_2 = \left|\frac{v}{\omega_2}\tan\beta\right| \tag{14b}$$

The semi-length l of the generatrix is the solution of equation (15), obtained after using Eq. 14b and eliminating η from equations showed in Fig. 4.

$$\frac{l\omega_2 \cos\vartheta}{v\tan\beta} + \tan\left(\frac{l\omega_2 \sin\vartheta}{v} - \pi\right) = 0 \tag{15}$$

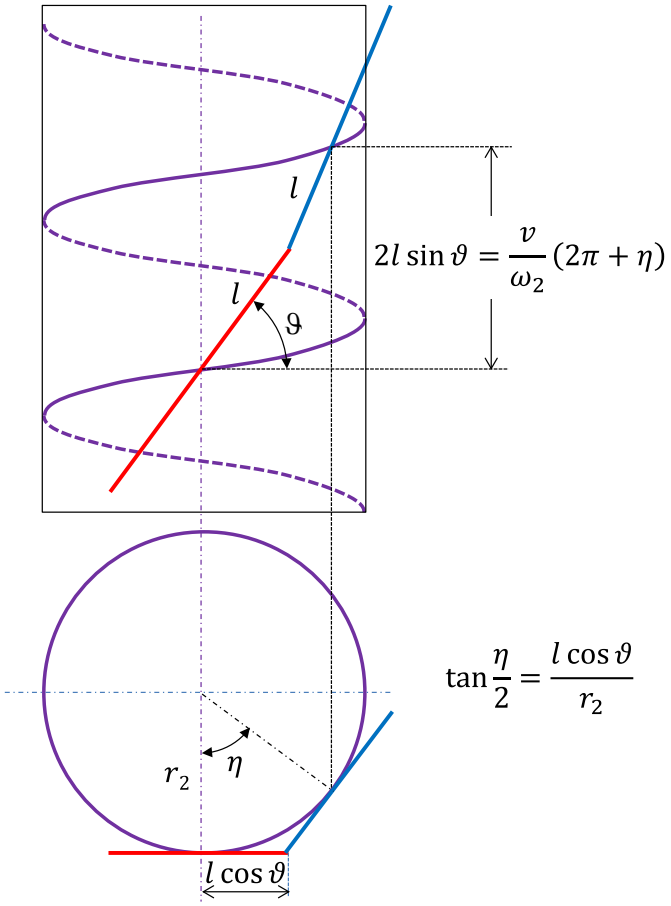

Fig. 4. Front and top views of the helix in which the helicoid is based, and two of its adjoining generatrices. The generatrix semi-length is obtained by eliminating η from the showed equations and using eq. 14b

Fig. 5 shows the rolling surfaces corresponding to a rotary-helical transmission where $v = 0.1$, $\omega_2 = 2\pi$, $\omega_1 = 3\pi$, and $\beta = 7\pi/4$ (in S.I. units). These values determine the distance between axes, which is d = 31 mm. In this case, the hyperboloid throat radius is 15 mm, and that of the helicoid is 16 mm. (Note that the distance between axes is equal to the sum of the throat radii).

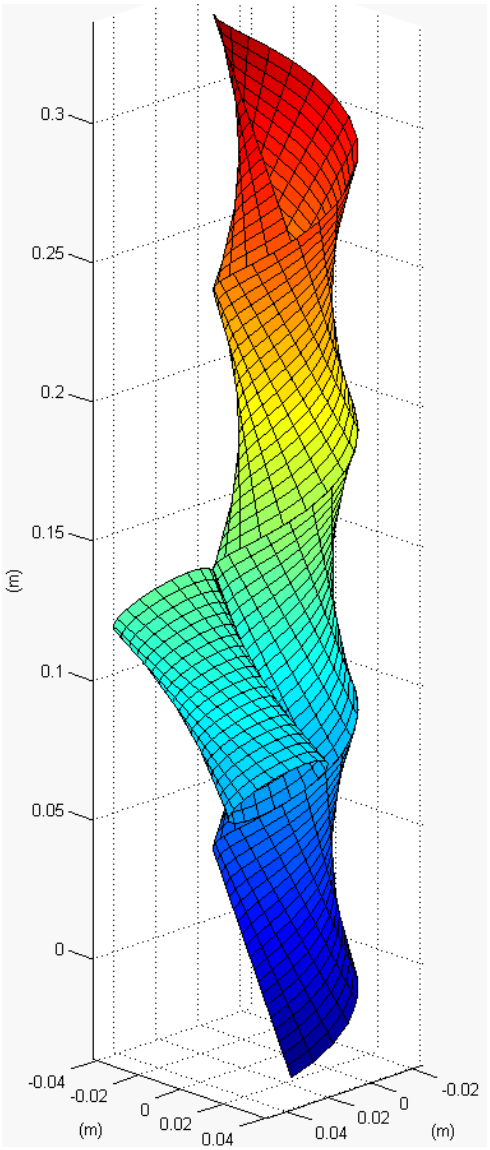

Fig. 5. The rotary-to-helical transmission rolling surfaces for the case: $\boldsymbol{v = 0.1}$, $\boldsymbol{\omega_1 = 3\pi}$, $\boldsymbol{\omega_2 = 2\pi}$, and $\boldsymbol{\beta = 7\pi/4}$ (S.I. units).

3. Examples of Different Rolling Surfaces for Rotary to Helical Transmission

Depending on the kinematic properties of the transmission, different geometries of rolling surfaces are found, although some of which would be impossible to implement practically.

First, the two cases containing singularities are discussed. One occurs when both axes are parallel to each other, that is, when $\beta = \frac{\pi}{2}$, which implies that $v = 0$ and corresponds to the traditional rotary-to-rotary transmission between parallel axes, where both rolling surfaces are cylinders. The other singularity occurs when the generatrix line is perpendicular to z-axis ($\vartheta = 0 \Rightarrow \beta = \sin^{-1}\frac{\omega_2}{\omega_1}$). In this case the ruled helicoid degenerates, and additionally $d = 0$.

Other cases that are impossible to implement occur when both surfaces intersect, albeit tangent to each other along their common generatrix line.

In Fig. 6 five sets of rolling surfaces are shown for $\omega_1 = \omega_2 = 2\pi\ rad/s$, $v = 0.1m/s$, with different values of β and are labeled a) to e) to facilitate their reference.

For cases a) and b) (where $\beta < \pi$) it is seen that the rolling surfaces intersect. However, when $\pi < \beta < 3\pi/2$ (as in case c)), d < 0 and the hyperboloid is then "behind" the helicoid. Finally, when $3\pi/2 < \beta < 2\pi$ (cases d) and e)), d > 0 and the hyperboloid is now "in front of" the helicoid.

In Fig. 7, a further five rolling surfaces are shown. These have been generated for $\omega_1 = 2\pi\ rad/s\ ;\ \omega_2 = 4\pi\ rad/s$, $v = 0.1m/s$, and with the values of β previously used. Here it can be seen that since $\omega_1 < \omega_2$, the hyperboloid throat diameter is greater than that of the helicoid. In fact, when $\beta < \pi$ (case a)), contact takes place on the interior surface of the hyperboloid.

Finally, in Fig. 8, five further rolling surfaces are shown, which have been generated for $\omega_1 = 4\pi\ rad/s\ ;\ \omega_2 = 2\pi\ rad/s$ (and so $\omega_1 < \omega_2$), $v = 0.1m/s$, and for the same values of β. When $\beta < \pi$, contact now takes place on the interior surface of the helicoid. (In order to facilitate its visualization, the plot has been inclined towards the viewer).

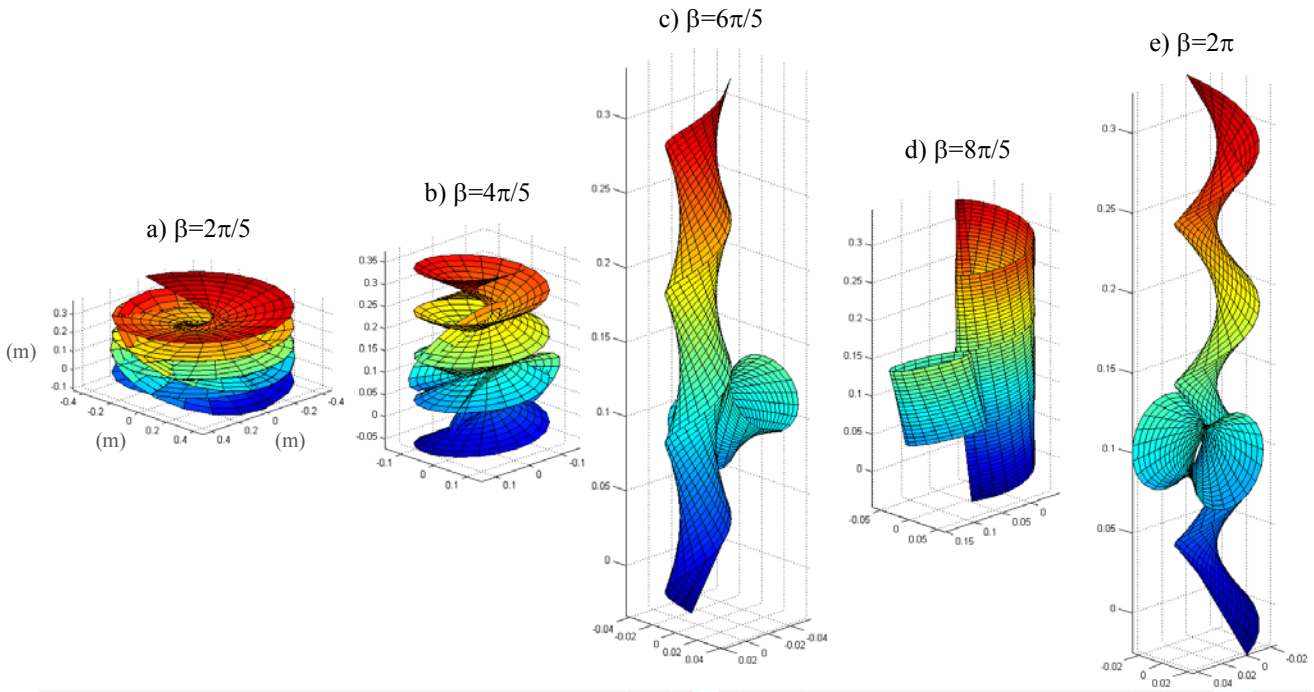

Fig. 6. The rolling surfaces for $\boldsymbol{\omega_1 = \omega_2 = 2\pi\ rad/s}$, $\boldsymbol{v = 0.1m/s}$, and $\boldsymbol{\beta = \frac{2\pi}{5}, \frac{4\pi}{5}, \frac{6\pi}{5}, \frac{8\pi}{5}, 2\pi}$.

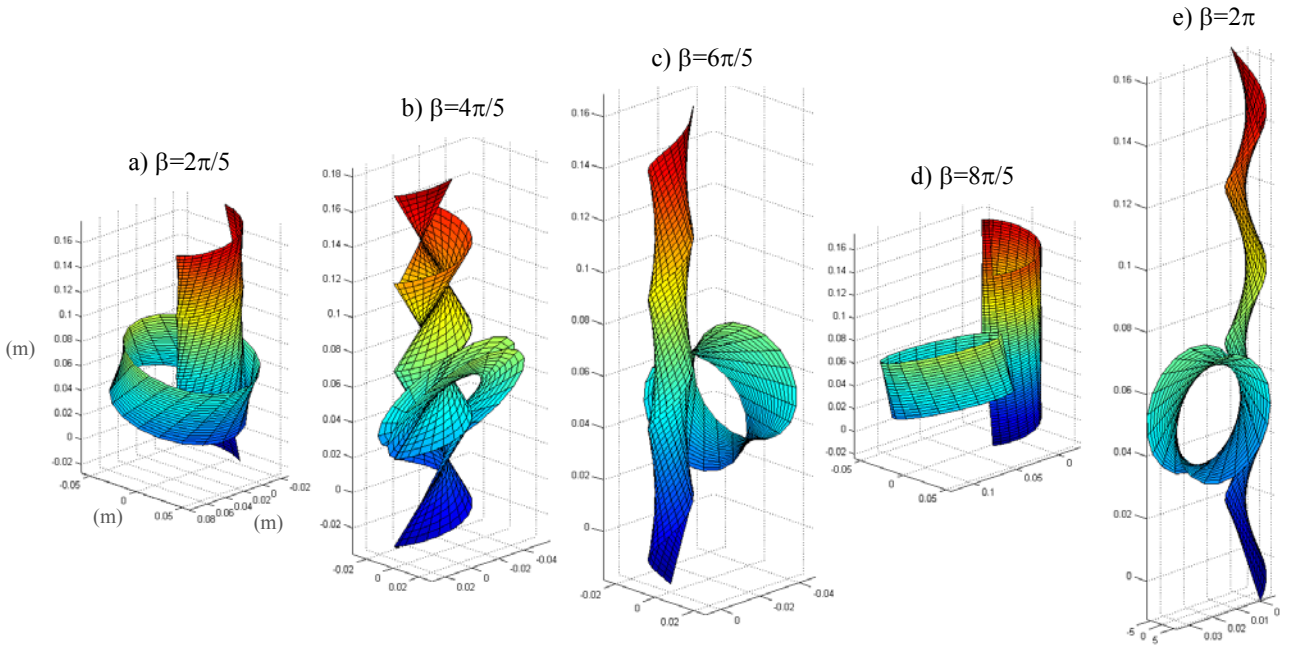

Fig. 7. The rolling surfaces for $\boldsymbol{\omega_1 = 2\pi\ rad/s, \omega_2 = 4\pi\ rad/s}$, $\boldsymbol{v = 0.1m/s}$, and $\boldsymbol{\beta = \frac{2\pi}{5}, \frac{4\pi}{5}, \frac{6\pi}{5}, \frac{8\pi}{5}, 2\pi}$.

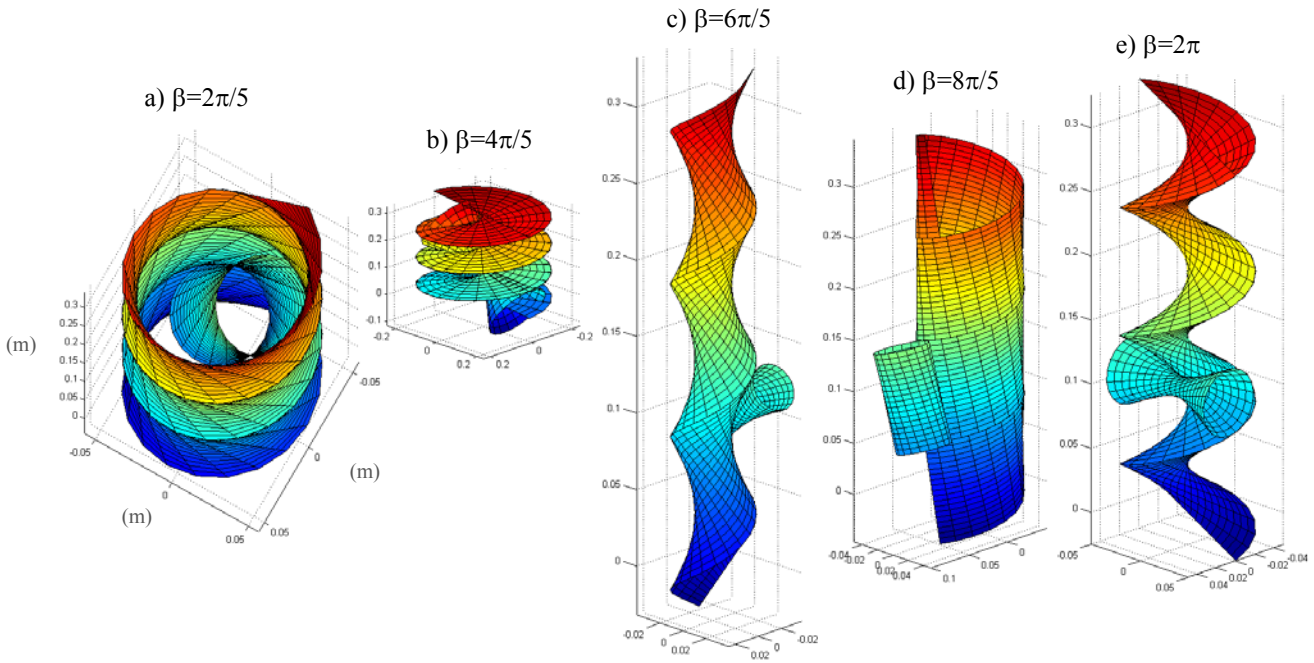

Fig. 8. The rolling surfaces for $\boldsymbol{\omega_1 = 4\pi\ rad/s, \omega_2 = 2\pi\ rad/s}$, $\boldsymbol{v = 0.1m/s}$, and $\boldsymbol{\beta = \frac{2\pi}{5}, \frac{4\pi}{5}, \frac{6\pi}{5}, \frac{8\pi}{5}, 2\pi}$.

4. Boolean Procedure for Gear Tooth Forming. Obtaining a Prototype for 3D Printing

In order to practically implement the kinematic pair described, first the toothed hyperboloid was modeled with a CAD program as a ruled surface between two identical involute gear profiles on two parallel planes at a distance $L = 2l \sin\vartheta \cos(\beta - \vartheta)$, shifted by the corresponding angle ξ (as shown in Fig. 9):

$$\xi = 2\tan^{-1}\left[\frac{L}{r_1}\tan(\beta - \vartheta)\right] \tag{16}$$

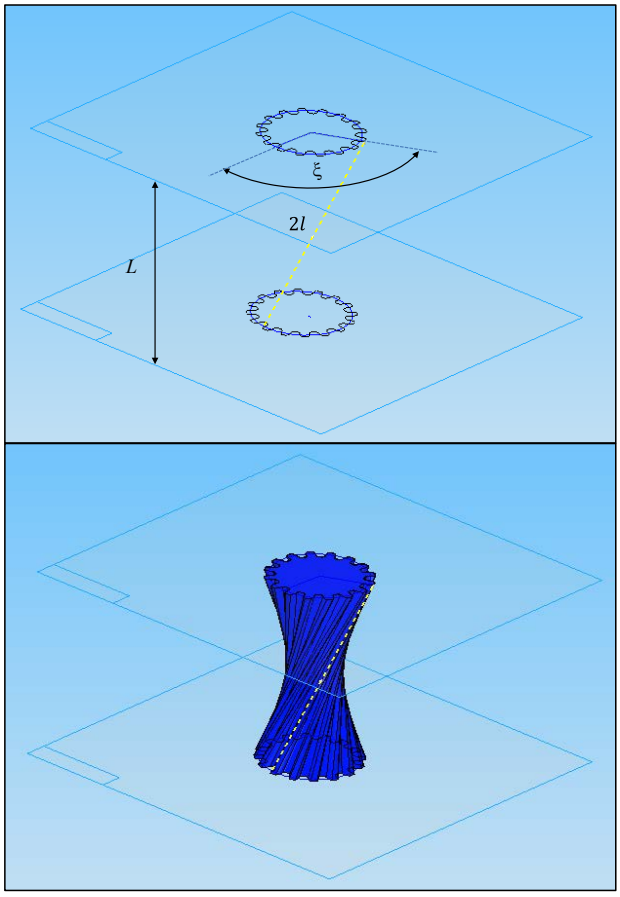

Fig. 9. Obtaining the toothed hyperboloid using a CAD program.

The conjugated toothed ruled helicoid was then obtained after a series of CAD Boolean subtractions (see Fig. 10a): the interference between the toothed hyperboloid (blue) and a wide cylinder (red), is removed from the latter. Between two consecutive subtractions, the corresponding increments were applied: the toothed hyperboloid rotates by an angle of $\omega_1 \Delta t$, whereas the cylinder rotates by an angle of $\omega_2 \Delta t$, and translates by an amount of $v \Delta t$. The resulting toothed helicoid shown in Fig. 10 (b) was obtained after more than 200 of such operations.

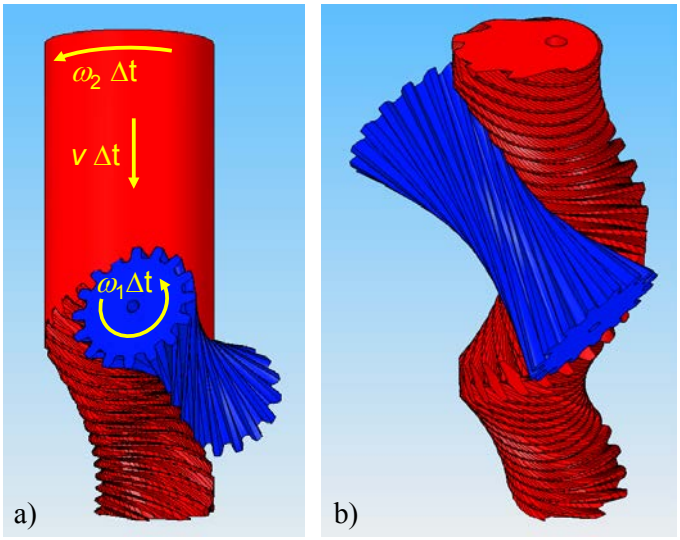

Fig. 10. a) Obtaining the toothed helicoid by a series of CAD Boolean subtractions and incremental motions between them. b) The resulting toothed helicoid (red).

Both gears have been physically produced using a 3D printer, and the assembly is shown in Fig. 11. Following this procedure, although the generated tooth flank turns out to be facetted, for a sufficiently small increment Δt, the level of faceting is negligible even for the highest resolution of the 3D printer (0.1 mm).

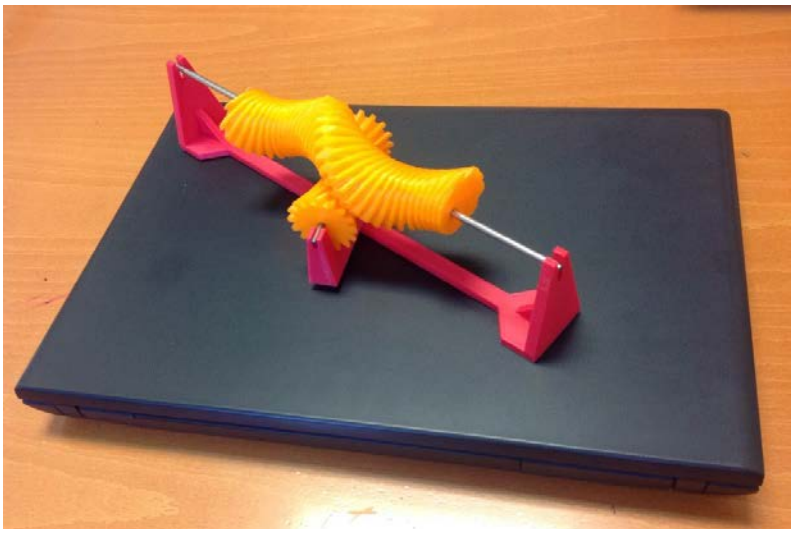

Fig. 11. The gear assembly produced on a 3D printer.

As it has been verified, the prototype presents negligible clearances and backlash, high reversibility, as well as continuous gearing without interference.

5. Meshing Equation for a Simple Generating Surface

In order to obtain an analytical meshing equation, a simple generating surface on the pitch hyperboloid has been taken into account: the ruled surface between two radio segments at both hyperboloid bases. This is also the right helicoid limited by two hyperboloids parallel to each other and parallel to the pitch hyperboloid (see Fig. 12).

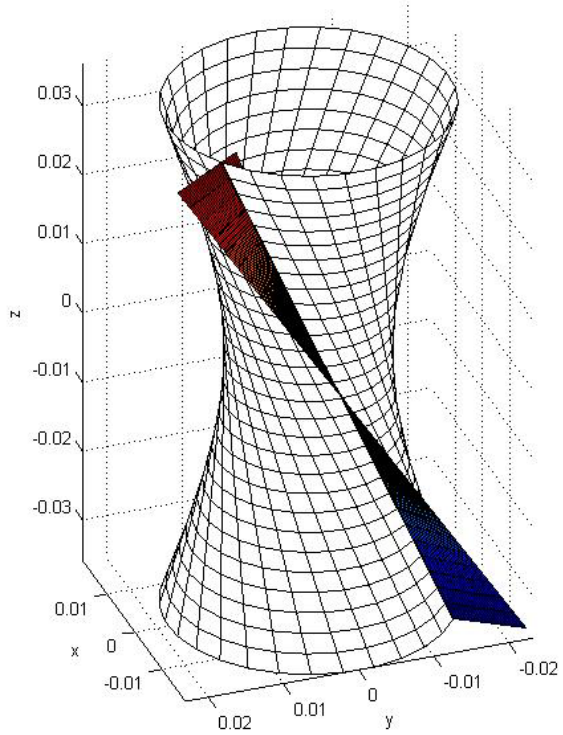

Fig. 12. The used generating surface on the hyperboloid: the ruled surface between two radio segments at its both bases.

This surface, has the following *s*,*p*-parametic equations, in the coordinate system rigidly connected to the hyperboloid:

$$\begin{cases} \mathrm{x_{s,p}} = -\mathrm{p}\cdot\cos(\xi/2) \\ \mathrm{y_{s,p}} = \mathrm{p}\cdot\mathrm{s}\cdot\sin(\xi/2) \\ \mathrm{z_{s,p}} = \mathrm{s}\cdot\mathrm{l}\cdot\cos(\beta-\vartheta) \end{cases} \tag{17}$$

Using homogeneous coordinates, $\boldsymbol{r}_{s,p} = \begin{pmatrix} x_{s,p} & y_{s,p} & z_{s,p} & 1 \end{pmatrix}^T$, and transformation matrices given in the Appendix, the *t*-family of surfaces is expressed in the coordinate system rigidly connected to the helicoid as:

$$\mathrm{r_{s,p,t}^{(h)}} = \mathrm{TR_{z(vt,\omega_2 t)}}\cdot\mathrm{TR_{x\left(-d,\frac{\pi}{2}-\beta\right)}^{-1}}\cdot\mathrm{R_{z(\omega_1 t)}^{-1}}\mathrm{r_{s,p}} \tag{18}$$

Then the meshing equation $\left[\frac{\partial \boldsymbol{r}^{(h)}}{\partial s} \;\; \frac{\partial \boldsymbol{r}^{(h)}}{\partial p} \;\; \frac{\partial \boldsymbol{r}^{(h)}}{\partial t}\right] = 0$, leads to an expression of the type shown in equation (19).

$$\mathrm{A(s,t)p^2 + B(s,t)p + C(s,t) = 0} \tag{19}$$

Where:

$$\begin{aligned} A &= \omega_2 \cos\tfrac{\xi}{2}\sin\tfrac{\xi}{2}\cos\beta\left[\cos\tfrac{\xi}{2}\cos\omega_1 t + s\sin\tfrac{\xi}{2}\sin\omega_1 t\right], \\ B &= l\cos(\beta-\vartheta)\,(\omega_1 - \omega_2\sin\beta)(\cos^2\beta + s^2\sin^2\beta) - v\tfrac{\omega_2}{\omega_1}\cos\tfrac{\xi}{2}\sin\tfrac{\xi}{2}, \\ C &= l^2 s\omega_2\cos\beta\cos^2(\beta-\vartheta)\left[\cos\tfrac{\xi}{2}\sin\omega_1 t - s\sin\tfrac{\xi}{2}\cos\omega_1 t\right] + \\ &+ lv\tfrac{\cos(\beta-\vartheta)}{\cos\beta}\left(\tfrac{\omega_2}{\omega_1}\sin\beta - 1\right)\left[\cos\tfrac{\xi}{2}\cos\omega_1 t + s\sin\tfrac{\xi}{2}\sin\omega_1 t\right] \end{aligned} \tag{20}$$

From equation (19), the parameter *p* can be easily eliminated when expressed in terms of *s* and *t*. Thus the envelope is calculated as the surface defined by parameters *s* and *t*:

$$\mathrm{e_{s,t}^{(h)}} = \mathrm{r_{s,p(s,t),t}^{(h)}} \tag{21}$$

In Fig. 13 left, some elements of the *t*-family of generating surfaces, as the hyperboloid moves, are represented in the system of reference rigidly connected to the helicoid. The corresponding envelope is shown in Fig. 13 right.

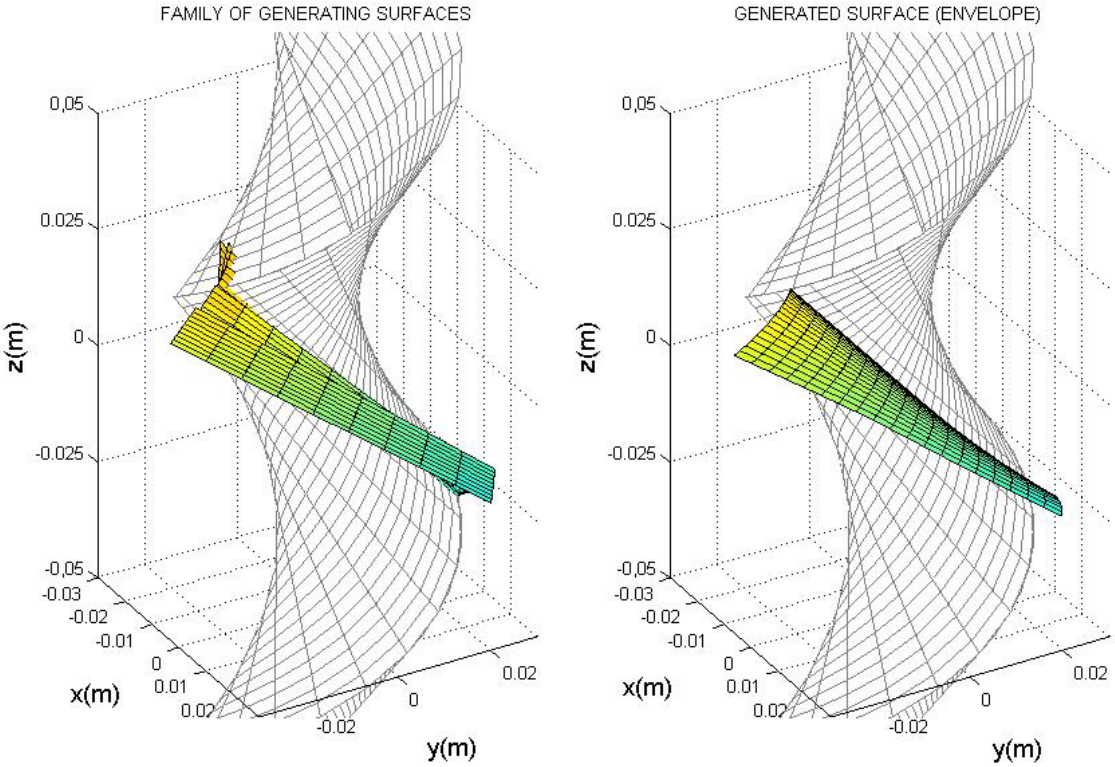

Fig. 13. Left: some elements of the family of generating surfaces belonging to the hyperboloid, in relative motion with respect to the helicoid (also shown). Right: the corresponding generated surface on the helicoid, as the envelope of the aforementioned family.

6. Conclusions and Future Work

In this manuscript, a rolling-joint higher kinematic pair that converts between rotary and helical motion has been presented and investigated.

Among the advantages of the transmission proposed, it can be mentioned that it is a simple and compact, one degree of freedom gear transmission, which prevents the undesirable locking, as it shows low friction and high reversibility.

The possible application fields include linear actuation and positioning, specific cutting tool motion (as in the automatic device for skin biopsy), and helical positioning in edge and radial relief sharpening tasks on helical tools

An algorithm that calculates and plots the rolling surfaces (pitch surfaces) for any set of transmission parameters has been developed, and was used to analyze several cases with several sets of defining parameters. The algorithm also calculates and plots a simple generating surface on the rotary gear (hyperboloid), and the corresponding generated surface on the helical gear (helicoid), for any set of transmission parameters.

The toothed gears were first modeled virtually with a CAD program, and then physically produced on a 3D printer. The prototype presents useful performances.

This paper deals only kinematic and topological aspects, but many other related aspects remain to be investigated such as the dynamics, power losses and efficiency, stress-strain calculations, manufacturing issues. Significant progress in analytical models are being made that will allow us to define the most suitable experimental system to get more reliable measurements, and define appropriate ranges for the variables involved. Other future line of research includes using the proposed rotary-linear gear transmission as the basis of linear actuators.

Appendix: Derivation of the *s*,*t*-parametric equations for the rotary-helical transmission pitch surfaces. Coordinate transformation matrices

These equations were required in Section II. The generatrix G in equations (11) can be expressed as a function of the parameter *s* as follows:

$$\begin{cases} x_{s,0} = -\dfrac{v}{\omega_2}\tan\beta \\ y_{s,0} = s \\ z_{s,0} = s\left(\tan\beta - \dfrac{\omega_2}{\omega_1\cos\beta}\right) \end{cases} \tag{A1}$$

Now we consider two Cartesian systems: $S(O,x,y,z)$, depicted in Fig.2, and $S'(O',x',y',z')$, so that the *x'* axis coincides with the *x*-axis and the *z'*-axis coincides with the axis of pure rotation, R. Then the transformation between them ($S \rightarrow S'$) is composed of a translation in the x direction by an amount *d*, followed by a rotation of angle $\pi/2-\beta$ about the *x*-axis. Using homogeneous coordinates [11,12]:

$$g_{s,0} = (x_{s,0} \quad y_{s,0} \quad z_{s,0} \quad 1)^T, \tag{A2}$$

the corresponding coordinate transformation matrix, is:

$$TR_{x\left(-d,\frac{\pi}{2}-\beta\right)} = \begin{pmatrix} 1 & 0 & 0 & -d \\ 0 & \sin\beta & -\cos\beta & 0 \\ 0 & \cos\beta & \sin\beta & 0 \\ 0 & 0 & 0 & 1 \end{pmatrix} \tag{A3}$$

Therefore, the parametric equations of the generatrix expressed in the *S'* coordinate system, are:

$$g'_{s,0} = TR_{x\left(-d,\frac{\pi}{2}-\beta\right)} g_{s,0} \tag{A4}$$

Next, we obtain the *s*,*t*-parametric equations of the hyperboloid in the *S'* coordinate system by applying a rotation about the *z'*-axis of angle $\omega_1 \cdot t$, the corresponding transformation matrix being

$$R_{z(\omega_1 t)} = \begin{pmatrix} \cos\omega_1 t & -\sin\omega_1 t & 0 & 0 \\ \sin\omega_1 t & \cos\omega_1 t & 0 & 0 \\ 0 & 0 & 1 & 0 \\ 0 & 0 & 0 & 1 \end{pmatrix} \tag{A5}$$

Hence:

$$g'_{s,t} = R_{z(\omega_1 t)} g'_{s,0} \tag{A6}$$

Finally, we return to the coordinates in the *S* system by applying the inverse of the first transformation ($S' \rightarrow S$), so the matrix is the inverse of (A3):

$$TR^{-1}_{x\left(-d,\frac{\pi}{2}-\beta\right)} = TR_{x\left(d,\beta-\frac{\pi}{2}\right)} = \begin{pmatrix} 1 & 0 & 0 & d \\ 0 & \sin\beta & \cos\beta & 0 \\ 0 & -\cos\beta & \sin\beta & 0 \\ 0 & 0 & 0 & 1 \end{pmatrix} \tag{A7}$$

From this we obtain:

$$g_{s,t} = TR_{x\left(d,\beta-\frac{\pi}{2}\right)} g'_{s,t} \tag{A8}$$

The matrix corresponding to these three successive coordinate transformations is the following matrix product:

$$M_R TR_{x\left(d,\beta-\frac{\pi}{2}\right)} R_{z(\omega_1 t)} TR_{x\left(-d,\frac{\pi}{2}-\beta\right)} =$$

$$= \begin{pmatrix} \cos\omega_1 t & -\sin\omega_1 t \sin\beta & \sin\omega_1 t \cos\beta & d(1-\cos\omega_1 t) \\ \sin\omega_1 t \sin\beta & \cos\omega_1 t \sin^2\beta + \cos^2\beta & \sin\beta\cos\beta\,(1-\cos\omega_1 t) & -d\sin\omega_1 t \sin\beta \\ -\sin\omega_1 t \cos\beta & \sin\beta\cos\beta\,(1-\cos\omega_1 t) & \cos\omega_1 t \cos^2\beta + \sin^2\beta & d\sin\omega_1 t \cos\beta \\ 0 & 0 & 0 & 1 \end{pmatrix} \tag{A9}$$

By multiplying this matrix by the column vector $\boldsymbol{g}_{s,0}$ and using equation (10)**,** the *s*,*t*-parametric equations of the hyperboloid in the *S* coordinate system (12) are obtained.

In order to obtain the *s*,*t*-parametric equations of the corresponding ruled helicoid, only a translation in the *z*-axis by an amount *vt*, and a rotation about the *z*-axis by an angle $\omega_2 t$ are required. The corresponding transformation matrix is then:

$$M_H = TR_{z(vt,\omega_2 t)} = \begin{pmatrix} \cos\omega_2 t & -\sin\omega_2 t & 0 & 0 \\ \sin\omega_2 t & \cos\omega_2 t & 0 & 0 \\ 0 & 0 & 1 & vt \\ 0 & 0 & 0 & 1 \end{pmatrix} \tag{A10}$$

By multiplying this matrix by the column vector $\boldsymbol{g}_{s,0}$**,** the *s*,*t*-parametric equations of the helicoid in the *S* coordinate system (13) are obtained.

Acknowledgment

The authors acknowledge the Spanish Found through the project "MAQSTATUS", DPI 2015-69325-C2-1-R, for financial support.

The authors also would like to thank David K. Anthony for technical help with English.

References

[1] Edison T.A. Phonograph or Speaking Machine. US Patent Office, No. 200,521. 1878.

[2] Grillo E., Vañó S., Jaén P., Castejón C., Meneses J., García-Prada, J.C., Rubio H. Dispositivo Automático para Biopsias Cutáneas. Oficina Española de Patentes y Marcas, No. ES2537831 B1 (12.06.2015). Int. Class.: A61B10/02 (2006.01). 2015.

[3] Harding W. Adjustable Angle Helix Generator for Edge and Radial Relief Sharpening. United States Patent, No. 3,600,860. 1971.

[4] Kwon H. and Fujimoto Y. FEM Analysis of High Thrust Spiral Motor. Advanced Motion Control, 2004. AMC'04. The 8th IEEE International Workshop on. pp. 635-640. 2004.
DOI: 10.1109/AMC.2004.1297943.

[5] Smadi I.A., Omori H, Fujimoto Y. On Direct-Drive Motion of a Spiral Motor. IECON 2010 - 36th Annual Conference on IEEE Industrial Electronics Society. pp. 927-932. 2010.
DOI: 10.1109/IECON.2010.5675163.

[6] Kominami T., Fujimoto Y. Studies on Thrust Characteristics of High-Thrust Spiral Motor. Electrical Engineering in Japan, Vol. 177, No. 2, 2011.
DOI: 10.1002/eej.21168.

[7] Caruso M., Cecconi V., Di Dio V., Di Tomasso A.O., Genduso F., La Cascia D., Liga R., Miceli R. Speed Control of a two-Degrees of Freedom Motor with Rotor Helical Motion for Industrial Applications. AEIT Annual Conference – From Research to Industry: The Need for a More Effective Technology Transfer, 2014. pp. 1-6. 2014.
DOI: 10.1109/AEIT.2014.7002051.

[8] Litvin F.L. and Fuentes A. Gear Geometry and Applied Theory. Cambridge University Press, 2004.

[9] Radzevich S.P. Theory of Gearing. Kinematics, Geometry and Synthesis. CRC Press, 2013.

[10] Giaquinta M. and Modica G. Mathematical Analysis. Linear and Metric Structures and Continuity . Birkhäuser, Boston. 2007.

[11] Denavit J. and Hartenberg R.S. A Kinematic Notation for Lower Pair Mechanisms Based on Matrices. Journal of Applied Mechanics. Vol. 22. No. 2, pp. 215-221. 1955.

[12] Litvin, F.L. Application of Matrices and Dual Number Calculations to Analysis of Spatial Gears. Proceedings of Leningrad Politekhnik Institute. No. 182. 1955.